Damaris Hecht*, Ingrid Ullmann, Daniel Oppelt, Tim Pfahler, Nadia Amer and Martin Vossiek

Millimeter-wave imaging and near-field spectroscopy for burn wound assessment

https://doi.org/10.1515/freq-2022-0100
Received May 9, 2022; accepted June 30, 2022;
published online August 15, 2022

Abstract: Diagnostic applications for skin in the microwave range have developed significantly in recent years, due the non-invasiveness of these applications and their ability to assess tissue water content. Despite their capabilities, however, there is still no appropriate clinically applicable microwave tool for the assessment of burn wounds. A common practice is the visual inspection and evaluation of burns by the doctor, which is a challenging task even for experienced medical professionals. An incorrect assessment can have far-reaching consequences, such as unnecessary surgery or surgery that is necessary but omitted. In this paper, two different approaches of millimeter-wave burn wound assessment are presented: millimeter-wave imaging and near-field spectroscopy. For imaging, a MIMO sparse array was used to assess *ex vivo* burns on porcine skin in the frequency range of 70–80 GHz. With a resonant millimeter-wave near-field probe, reflective spectroscopy at individual sites of an *ex vivo* burn on porcine skin in the frequency range of 75–110 GHz was performed. The results showed individual advantages and drawbacks for both approaches, with surprising benefits of the spectroscopic method. Nevertheless, both approaches were shown to be suitable for clinical usage in diagnosing burns.

Keywords: burn injuries; millimeter-wave imaging; millimeter-wave spectroscopy; near-field probe; reflectometry.

1 Introduction

Burns are thermal damage to the skin that can be caused in various ways, ranging from a self-healing sunburn to a highly painful wound requiring medical treatment to a life-threatening injury. The right assessment and the appropriate treatment of a burn are key to a successful therapy that both sustains life and improves quality of life by lowering the risk of amputations and long-term effects such as motion limitations and scars. In clinical practice, to find the right treatment, the burn injury is inspected visually. To help with the assessment, it is clinical practice that the burn is categorized according to four different burn degrees and in addition, the affected skin area is estimated in proportion to the whole body surface. The degree of burn connects the appearance of the burn with its depth and thus reveals the extent of damage of the skin layers. The main signs and characteristics for the individual burn degrees are listed in Table 1. The decision of the doctor whether the burn injury can heal by itself or needs surgical treatment like removing necrotic tissue and skin transplantation is based on the degree of the burn. Even though burns seem to have a clearly visible signature, evaluating them correctly is a challenge. And in particular the classification into degree II a or b has severe consequences if decided incorrectly. Unnecessary or missed surgery is usually only recognized too late in the course of the healing process. Consequentially, there is great need for a supporting technical system, e.g. an imaging system, to avoid false burn classifications.

Developments in the field of microwave technologies over the past few years to decades have shown promise for a wide range of medical diagnostics: breast cancer tomography [1–3], skin cancer detection [4, 5], and the non-invasive measurement of blood glucose level [6, 7], to name just a few. In the area of burn wound assessment, several research groups have made promising advances, mainly in the form of imaging and reflectometry techniques. Owda et al. focused on millimeter-wave emissivity metric [8, 9] as a passive method for burn evaluation, but also conducted synthetic aperture (SAR) imaging [10]. A combination of reflectometric near-field probing and imaging was conducted by the research group of Gao et al. [11, 12]. Oppelt et al. focused on imaging with a MIMO SAR system [13] as well as imaging with a near-field probe [14]. While the reflectometry approaches tend to be more targeted at the determination of skin properties [15, 16] than on developing a clinically applicable tool, the imaging methods

***Corresponding author: Damaris Hecht**, Institute of Microwaves and Photonics (LHFT), Friedrich-Alexander-Universität Erlangen-Nürnberg (FAU), Erlangen, Germany, E-mail: damaris.hecht@fau.de
Ingrid Ullmann, Daniel Oppelt, Tim Pfahler, Nadia Amer and Martin Vossiek, Institute of Microwaves and Photonics (LHFT), Friedrich-Alexander-Universität Erlangen-Nürnberg (FAU), Erlangen, Germany, E-mail: ingrid.ullmann@fau.de (I. Ullmann), daniel.oppelt@fau.de (D. Oppelt), tim.m.pfahler@fau.de (T. Pfahler), nadia.amer@fau.de (N. Amer), martin.vossiek@fau.de (M. Vossiek)

Table 1: Main characteristics of the different degrees of burn. The assignment to a burn degree helps with the decision for the right treatment.

Degree of burn	Visual impression	Affected skin layers	Pain sensation	Healing process
I	Redness	Epidermis	Light pain	Healing by itself
II (Partial burns)				
a	Blisters, swelling, moisture	Epidermis, superficial dermis	Strong pain	Healing by itself
b	Yellow or white areas, may be blisters	Epidermis, deep dermis	Less pain	Scars are probable, skin transplantation may be required
III (full thickness burn)	Brown/white/black color	Epidermis, dermis, subcutis	Little to no pain	Skin transplantation required
IV	Black	All skin layers and underlying tissues like muscle, bone	Painless	Surgical treatment, amputations

have proven to be particularly suitable for monitoring the healing process of burn wounds through dressing [8, 17]. Moreover, Rangaiah et al. recently presented a resonant microwave sensor for burn degree assessment [18]. But overall, resonant designs are underrepresented in the field of burn wound evaluation. Nevertheless, a resonant design is in our opinion underestimated: It is particularly sensitive to the water content and can provide distinct features for the machine-based classification of burn injuries. This makes it a highly recommended candidate for clinical use. Therefore, we designed a resonant near-field probe for reflective spectroscopic measurements presented in this study. Moreover, since the resonant near-field probing is more suitable for small burns, we also present a MIMO imaging system appropriate for large burns. It is real-time capable, what is also crucial for clinical use, and thereby is five times faster than the imaging system presented in previous studies [13].

Consequentially, in this paper, two different approaches in the millimeter-wave range for the assessment of burns are presented: MIMO imaging and resonant near-field spectroscopy. For the first method, imaging with a MIMO sparse array was performed in the frequency range 70–80 GHz, suitable for the fast assessment of large burns. For the second method, a resonant near-field probe is presented, which is suitable for small burns or the spot check assessment of burn sites whose classification is critical or unsure. With the probe, reflectivity measurements were conducted in the frequency range 75–110 GHz, which provide resonant spectra characteristic for the material being measured. Both methods were tested on *ex vivo* partially burned porcine skin, since the skin of pigs has similar properties to human skin and is easy to purchase. Furthermore, the comparability of the two methods presented is thereby ensured, as well as the comparability with the studies of other research groups, since the usage of porcine skin is state of the art for *ex vivo* testing on burns. Finally, the advantages and disadvantages of the two approaches were analyzed and evaluated for their suitability for everyday clinical practice.

2 Materials and methods for MIMO imaging

For the MIMO imaging of the partially burned porcine skin, the QAR imaging system of Rohde & Schwarz was used [19]. The QAR is appropriate for short range applications and consists of a sparse periodic array design with an architecture of 3×4 cluster units that each consists of 94 Tx (transmitting) and 94 Rx (receiving) antennas; see Figure 1 left for the cluster unit and Figure 1 right for the QAR setup. The array geometry is described in detail in [20], with the difference of a cluster arrangement of 4×4 clusters. The Tx and Rx antennas operate with a frequency-stepped continuous-wave (SFCW) signal in the frequency range 70–80 GHz. Compared to the imaging system used in previous studies [13], with an acquisition

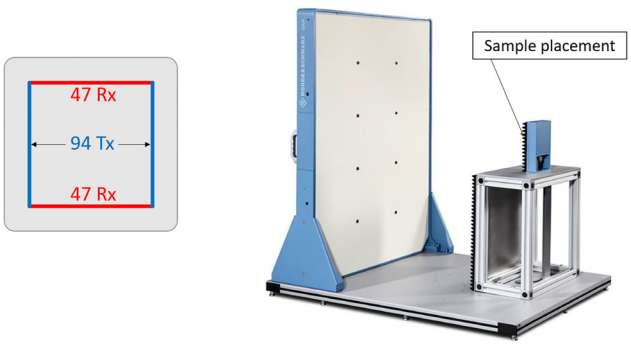

Figure 1: Left: subunit (cluster) with 94 transmitting antennas (Tx) and 94 receiving antennas (Rx) as part of the sparse periodic array used to make reflection images of partially burned *ex vivo* porcine skin; right: imaging setup [19].

time $\Delta t < 1$ s and a lateral resolution $\delta_{x,y} = 3$ mm, the imaging system used is more than five times faster and has a larger field of view (30 × 30 cm), while still having a sufficient resolution. As a result, the presented real-time imaging system is more suitable for clinical application for assessing burn wounds since it is less prone to movements of the patient.

The MIMO imaging was conducted on freshly extracted porcine skin, which was obtained directly from the slaughterhouse and contained the epidermis and dermis without the subcutaneous fat. The piece of skin, excised at the back or stomach area of the pig, measured 18 × 25 cm.

To demonstrate the full potential of the imaging system, the measurements were conducted with small burns of different degrees. This was achieved by treatment with a gas soldering iron (ERSA independent 130) without the use of a soldering tip at a 10 cm distance from the skin surface, which resulted in round shaped burns with a diameter of at least 1 cm, which increased gradually according to the degree of the burn. The heat exposure time was increased in 10 s steps to 40 s, resulting in four burns of different degree. One burn with an exposure time larger than 60 s was added. The porcine skin with the resulting burns is shown in Figure 2. For measurement, the porcine skin was fixated in the measurement setup on the sample placement holder with the surface parallel to the aperture plane.

3 Imaging results

In Figure 3, the measurement result of the MIMO imaging of the partially heat-treated *ex vivo* porcine skin is presented. The photo in Figure 3 left shows the porcine skin piece in whole size, with the five burns of different heat exposure times. Figure 3 right shows the corresponding imaging result with the pixel intensities representing the reflection coefficient Γ in %. As expected, areas with a high water content such as normal tissue appear bright in the grayscale radar image due to the high dielectric loss and consequentially high reflectivity of water. Whereas burned areas seem dark with low intensity in the image due to the low water content and consequentially low reflectivity. The difference between the particular burns is also visible: Burns with a heat exposure time less than 20 s are only lightly visible, whereas the burn after 30 s is clearer definable and the one after 40 s has an even higher contrast with the unburned tissue. A heat treatment longer than 60 s seems not to significantly increase the contrast with the surrounding tissue. Remarkably, there is also a bright halo around the burns with a treatment time of 30 s and longer, which suggests that there is more water present. It is assumed that this results from exudates, which arise at the edge of the burns during the burning process, as it was also observed in [8].

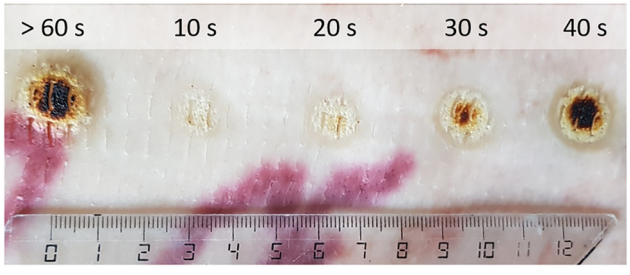

Figure 2: *Ex vivo* porcine skin treated with soldering iron heat. Exposure time to the heat was from left to right: More than 60 s, 10, 20, 30, and 40 s.

Although the different burn degrees can be distinguished in the radar image and therefore the potential as a burn assessment tool is demonstrated, there are areas on the unburned skin that differ from each other significantly in intensity. This is assumed to be the result of the uneven geometry of the skin surface leading to changes in the measured reflectivity due to a changing angle of the surface toward the antennas. As a consequence, the measured reflection cannot be safely attributed to an actual change of the reflection properties of the material, caused in burns by differing water content. This may prove challenging when aiming to use the technique as a reliable burn assessment tool.

4 Materials and methods for near-field spectroscopy

The near-field resonant probe for the spectroscopic measurements is based on a W-band rectangular waveguide (WR-10, cross-sectional width a = 2.54 mm, height b = 1.27 mm) with an integrated resonance chamber. In Figure 4, the CAD model of the probe design is shown. The resonance cavity is located at the probe tip and is coupled by a rectangular aperture with a width of a_{ap} = 2 mm and a height of b_{ap} = 0.5 mm. In the unloaded state, the probe is open-ended, which means that the second closure of the resonator is initially missing and then created later while measuring by placing the measurement object, i.e. the porcine skin, at the probe tip. The waveguide probe was 3D printed by stereolithography and silver-plated to gain conductivity. The slits in the sidewalls of the waveguide probe are a product of the silver-plating process [21]. The

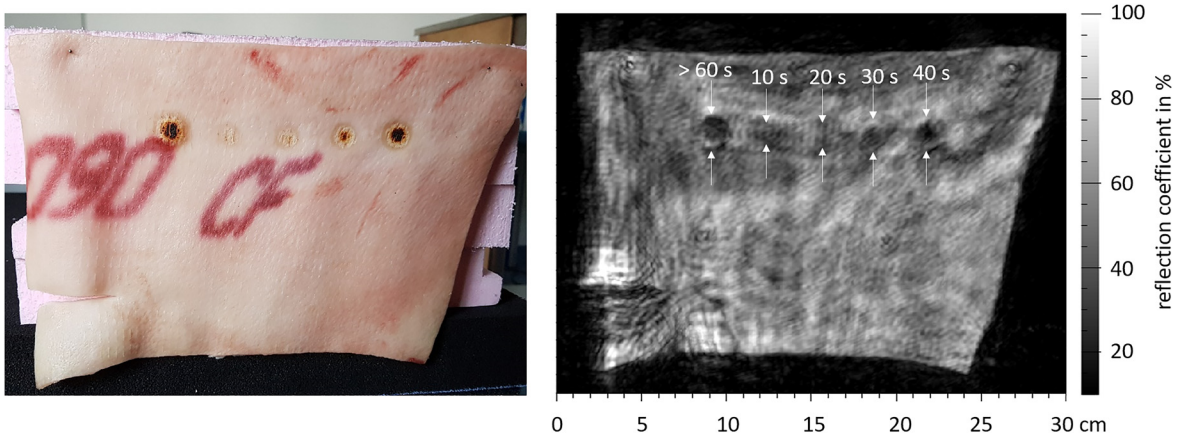

Figure 3: Left: photo of the piece of porcine skin with burns of different degree; right: radar image of the porcine skin. The burns are about 1 cm in diameter.

manufacturing via 3D printing enables small and complex designs, fast production, and easy reproducibility. The flange at the port of the waveguide was added to mount the probe in the measurement setup.

The resonance frequencies of a rectangular waveguide cavity [22] are in general given by

$$f_{mnl} = \frac{c}{2\pi\sqrt{\mu_r \varepsilon_r}} \sqrt{\left(\frac{m \cdot \pi}{a}\right)^2 + \left(\frac{n \cdot \pi}{b}\right)^2 + \left(\frac{l \cdot \pi}{d}\right)^2} \quad (1)$$

with the waveguide mode numbers m, n, l; the relative permeability μ_r, the relative permittivity ε_r, and the propagation speed c in the medium inside the cavity; and the cavity dimensions which are the width a, height b, and length d. Since the cavity of our probe design is filled with air, it can be approximated that $\mu_r = \varepsilon_r = 1$ and $c = c_0$, the speed of light in vacuum. For the in rectangular waveguides predominant H_{10} or TE_{10} mode, equation (1) then simplifies to

$$f_{10,l} = \frac{c_0}{2\pi} \sqrt{\left(\frac{\pi}{a}\right)^2 + \left(\frac{l\pi}{d}\right)^2}. \quad (2)$$

The spectroscopic measurements were conducted across the whole frequency band from 75 to 110 GHz. To have several resonant frequencies present in this frequency range, the length of the resonant cavity was chosen to be $d = 23.07$ mm, which resulted in seven resonant frequencies $f_{10,\,(l=8,\ldots,14)}$, listed in Table 2. The resonant mode numbers correspond with the number of electric field maxima along the propagation direction in the waveguide; the electric field view of $f_{10,14}$ with 14 electric field maxima is shown in Figure 5.

In the measurement setup, the probe is connected to a network analyzer to measure the reflection coefficient Γ

Table 2: Resonant mode number l and corresponding resonant frequencies of the chosen probe design that are visible in the measuring frequency range of 75–110 GHz.

l	8	9	10	11	12	13	14
$f_{10,l}$ in GHz	78.6	83.1	87.8	92.7	97.8	103.0	108.4

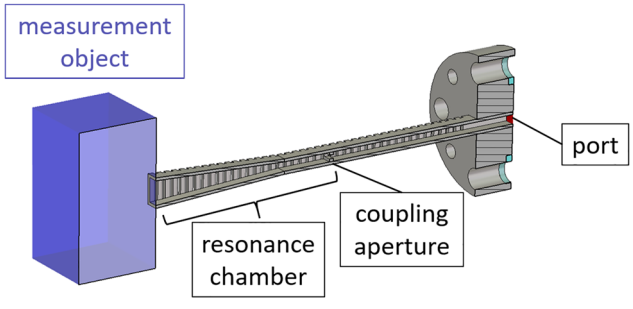

Figure 4: Length cut of the 3D CAD model of the resonant near-field WR-10 waveguide probe developed for spectroscopic measurements. The blue cuboid demonstrates the placement of the measurement object at the probe tip.

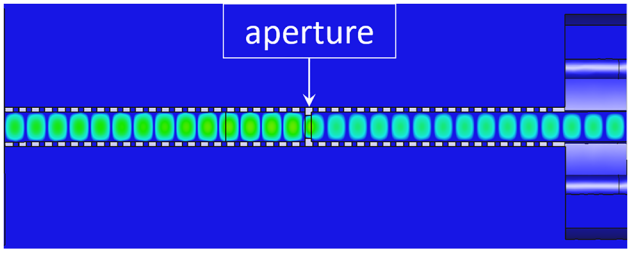

Figure 5: Electric field view of the resonant near-field probe at the 14th resonant frequency $f_{10,14}$ (view from above).

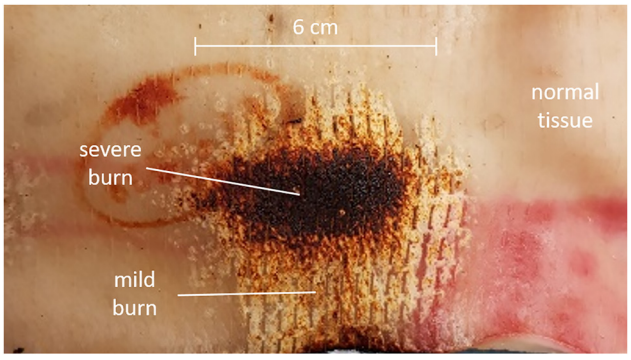

Figure 6: Burn with different areas of burn degree on porcine skin used for spectroscopic measurements with the presented near-field probe.

over the frequency range of 75–110 GHz. We used a Rohde & Schwarz ZVA-24 vector network analyzer and a Rohde & Schwarz ZVA-Z110 frequency converter for measurement. Since the measurement setup is realized as a 1-port measurement, the reflection coefficient is given by S_{11}. In the measured reflection spectra, the resonant show up as points with very low S_{11} values due to standing waves in resonant case. The Q factor at the single resonant frequencies changes according to the dielectric properties of the site under measurement, depending on the water content.

The porcine skin for the spectroscopic measurements was acquired in the same way as the one for the MIMO imaging. Using a commercial Bunsen burner, a burn with a diameter of about five to six cm was created, so that areas of different burn degree are present. A photo of the created burn is shown in Figure 6. For the measurements, the required site of the porcine skin was held onto the probe tip. Measurements were conducted of the middle of the burned area (severe burn, full thickness), of the peripheral area of the burn (mild burn), and of the unburned surrounding tissue (normal tissue). As a reference measurement, the resonance spectrum of water was measured as well with the probe. This was performed by holding a paper tissue soaked with tap water onto the probe tip.

5 Near-field spectroscopy results

The spectroscopic measurements that were performed on three areas of partially burned *ex vivo* porcine skin (see Figure 6) are presented in Figure 7, as well as the measured reference spectrum of water. Among the measured spectra, water has the highest Q factor of all data, present at the resonant frequency $f_{10,11} \approx 92.7$ GHz, which means that the resonator is best adjusted at this resonant frequency. That water has the highest Q factor of all spectra was to be expected because the probe design had been created to be sensitive to a high water content. For the burns, it is assumed that the burning process reduces the water content through evaporation and therefore, the water content

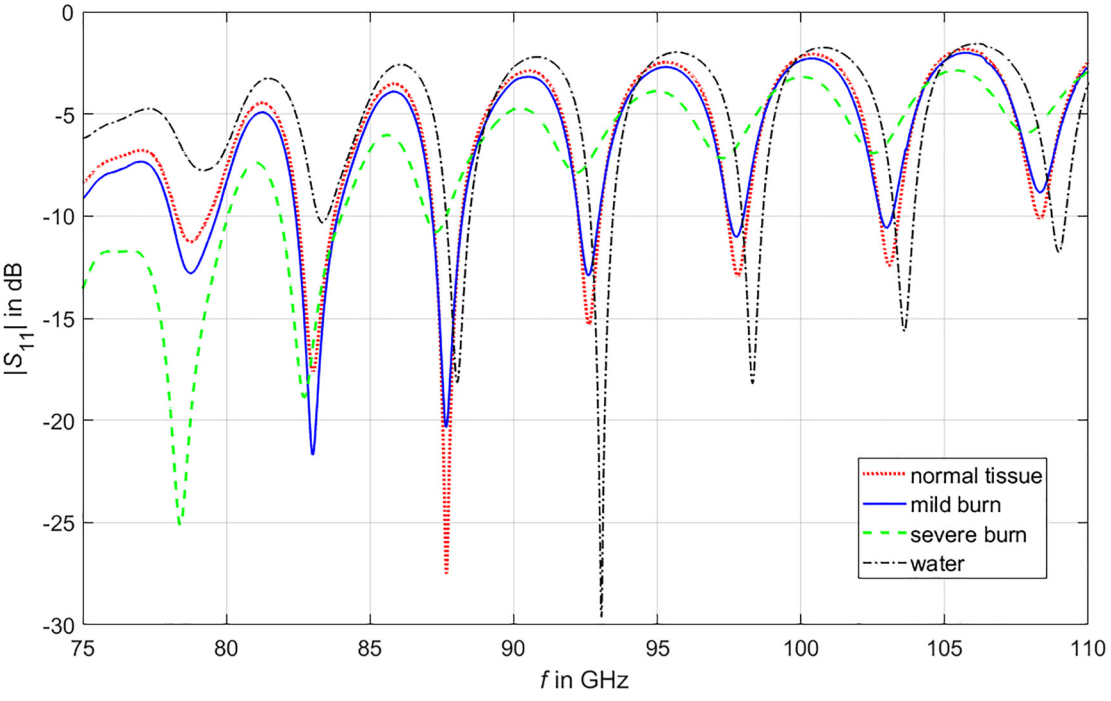

Figure 7: Reflection spectra of a severe burn site, a mild burn site, and normal (unburned) tissue measured with the resonant near-field probe on *ex vivo* porcine skin. The measurement of water was added for reference.

is understood to decrease in this order: normal tissue, mild burn, and severe burn. In Figure 7, it can be seen that the lower the water content of the sample, the lower the resonant frequency where the highest Q factor (global minimum of the curve) is present. This provides a specific distinguishing feature for the different samples, i.e., burn degrees. Furthermore, it is observable that in the frequency ranges between the resonant frequencies, the reflectivity decreases with the increasing absence of water in the sample, visible as a dip of the whole curve. This is to be expected due to the high reflectivity of water.

The presented measurements are example measurements; repetition of measurements led to slight variances in the Q factor. However, the characteristic feature, the resonant frequency where the highest Q factor developed, always stayed the same for a distinct material. Consequently, the materials are clearly distinguishable by the resonant frequencies, with the global minimum of the curve providing a suitable feature for a machine-based classification of burns. The suitability of the characteristic spectra for machine-based evaluation is an important property for clinical use as a burn wound diagnostic application and, moreover, is a possible advantage over other methods.

Furthermore, the measurements were performed with contact to the tissue but non-contact measurements are highly preferable for clinical practice; distant measurements with the near-field probe are possible but since the measurements are sensitive to the distance between probe tip and surface of the measuring object, it must be ensured that the same distance is always maintained and known to achieve comparability of the measurements. A distance of a few millimeters is possible.

6 Conclusions

In this paper, a millimeter-wave MIMO imaging system and a resonant near-field probe for spectroscopy that were used to assess different burn degrees on *ex vivo* partially burned porcine skin were presented. The two approaches were analyzed with respect to their suitability for clinical use as a burn evaluation tool. It was found that each approach has individual advantages and disadvantages. Both presented methods, imaging and spectroscopy, have an appropriate acquisition time for allowing real-time results. With the imaging system, it is possible to assess large burns at once and contactless. Nevertheless, there are uncertainties in the differentiation of light burn areas from unburned skin and the surface geometry of the skin influences the measured reflectivity and therefore cannot be attributed directly to the reflective properties of the measured burn site. The spectroscopy approach is appropriate for a spot-by-spot check up of critical burn areas. The method is convincing in how it is very sensitive to different degrees of burn and providing characteristics that are suitable for machine-based evaluation. In order to realize the full potential of the probe for clinical practice, the probe should be integrated into a system that ensures a constant distance from the burn wound.

Author contributions: All the authors have accepted responsibility for the entire content of this submitted manuscript and approved submission.
Research funding: We would like to thank Rohde & Schwarz very much for providing the QAR radar scanner to our institute. The presented studies were supported by the Deutsche Forschungsgemeinschaft (DFG, German Research Foundation) within the priority program electromagnetic sensors for life sciences (ESSENCE) under grant VO 1453/19–2.
Conflict of interest statement: The authors declare no conflicts of interest regarding this article.

References

[1] H. Bahramiabarghouei, E. Porter, A. Santorelli, B. Gosselin, M. Popović, and L. A. Rusch, "Flexible 16 antenna array for microwave breast cancer detection," *IEEE (Inst. Electr. Electron. Eng.) Trans. Biomed. Eng.*, vol. 62, no. 10, pp. 2516–2525, 2015.
[2] L. Wang, "Microwave sensors for breast cancer detection," *Sensors*, vol. 18, no. 2, p. 655, 2018.
[3] S. M. Salvador and G. Vecchi, "Experimental tests of microwave breast cancer detection on phantoms," *IEEE Trans. Antenn. Propag.*, vol. 57, no. 6, pp. 1705–1712, 2009.
[4] P. Mehta, K. Chand, D. Narayanswamy, D. G. Beetner, R. Zoughi, and W. V. Stoecker, "Microwave reflectometry as a novel diagnostic tool for detection of skin cancers," *IEEE Trans. Instrum. Meas.*, vol. 55, no. 4, pp. 1309–1316, 2006.
[5] F. Töpfer, S. Dudorov, and J. Oberhammer, "Micromachined 100GHz near-field measurement probe for high-resolution microwave skin-cancer diagnosis", in *2012 IEEE/MTT-S International Microwave Symposium Digest.*, IEEE, 2012, pp. 1–3.
[6] Y. Nikawa and T. Michiyama, "Blood-sugar monitoring by reflection of millimeter wave," in *2007 Asia-Pacific Microwave Conference*, IEEE, 2007, pp. 1–4.
[7] G. Guariti, M. Hofmann, R. Weigel, G. Fischer, and D. Kissinger, "Determination of sugar concentration in aqueous solutions using ultra-wideband microwave impedance spectroscopy", in *2013 IEEE MTT-S International Microwave Symposium Digest (MTT)*, IEEE, 2013, pp. 1–4.
[8] A. Y. Owda, N. Salmon, S. Shylo, and M. Owda, "Assessment of bandaged burn wounds using porcine skin and millimetric radiometry," *Sensors*, vol. 19, no. 13, p. 2950, 2019.
[9] A. Y. Owda, N. Salmon, S. W. Harmer, et al., "Millimeter-wave emissivity as a metric for the non-contact diagnosis of human skin conditions," *Bioelectromagnetics*, vol. 38, no. 7, pp. 559–569, 2017.

[10] A. Y. Owda, M. Owda, and N.-D. Rezgui, "Synthetic aperture radar imaging for burn wounds diagnostics," *Sensors*, vol. 20, no. 3, p. 847, 2020.
[11] Y. Gao and R. Zoughi, "Millimeter wave reflectometry and imaging for noninvasive diagnosis of skin burn injuries," *IEEE Trans. Instrum. Meas.*, vol. 66, no. 1, pp. 77–84, 2016.
[12] Y. Gao and R. Zoughi, "Millimeter reflectometry as an effective diagnosis tool for skin burn injuries," in *2016 IEEE International Instrumentation and Measurement Technology Conference Proceedings*, IEEE, 2016, pp. 1–5.
[13] D. Oppelt, J. Adametz, J. Groh, O. Goertz, and M. Vossiek, "MIMO-SAR based millimeter-wave imaging for contactless assessment of burned skin," in *2017 IEEE MTT-S International Microwave Symposium (IMS)*, IEEE, 2017, pp. 1383–1386.
[14] D. Oppelt, T. Pfahler, F. Distler, J. Ringel, O. Goertz, and M. Vossie, "Nearfield imaging probe for contactless assessment of burned skin," in *2017 European Radar Conference (EURAD)*, IEEE, 2017, pp. 195–198.
[15] Y. Gao, M. T. Ghasr, M. Nacy, and R. Zoughi, "Towards accurate and wideband in vivo measurement of skin dielectric properties," *IEEE Trans. Instrum. Meas.*, vol. 68, no. 2, pp. 512–524, 2018.
[16] A. Y. Owda, N. A. Salmon, and N.-D. Rezgui, "Electromagnetic signatures of human skin in the millimeter wave band 80–100 GHz," *Prog. Electromagn. Res. B*, vol. 80, pp. 79–99, 2018.
[17] D. Oppelt, P. Korf, J. Adametz, "Effects of different types of burn wounds and its dressings on millimeter-wave images," *Frequenz*, vol. 72, nos. 3–4, pp. 151–158, 2018.
[18] P. K. B. Rangaiah, B. Mandal, E. Avetisyan, "Preliminary analysis of burn degree using non-invasive microwave spiral resonator sensor for clinical applications," *Front. Med. Technol.*, vol. 4, 2022, https://doi.org/10.3389/fmedt.2022.859498.
[19] Rohde & Schwarz, 2022. Available at https://www.rohde-schwarz.com/us/products/test-and-measurement/radome-tester/rs-qar-quality-automotive-radome-tester_63493-553077.html.
[20] S. S. Ahmed, A. Schiessl, and L.-P. Schmidt, "A novel fully electronic active real-time imager based on a planar multistatic sparse array," *IEEE Trans. Microw. Theor. Tech.*, vol. 59, no. 12, pp. 3567–3576, 2011.
[21] K. Lomakin, M. Sippel, K. Helmreich, and G. Gold, "Design and analysis of 3d printed slotted waveguides for d-band using stereolithography and electroless silver plating," in *2020 IEEE/MTT-S International Microwave Symposium (IMS)*, IEEE, 2020, pp. 177–180.
[22] D. M. Pozar, *Microwave Engineering*, 2nd ed., John Wiley & Sons, 1998.